PAPER

Check for updates

Preparation of Fe₃O₄@CSAC catalyst and its degradation performance and heat release mechanisms in sewage degradation

Ke Zhang and Yuntao Yan [ID] *

To investigate the exothermic characteristics of a heterogeneous Fenton system during the degradation of organic sewage and provide technical support for energy recovery in sewage treatment, the catalyst Fe₃O₄@CSAC (coconut shell-activated carbon) was prepared. Subsequently, both the degradation performance and exothermic behaviour of the (Fe₃O₄@CSAC)–H_2O_2 heterogeneous Fenton-like system in the degradation of sewage were studied. The results demonstrated that the (Fe₃O₄@CSAC)–H_2O_2 heterogeneous Fenton-like system exhibited a high degradation rate for sewage and released a significant amount of heat during the degradation process, making it suitable for energy recovery through a sewage-source heat pump. These findings showed that the concentration of added Fe₃O₄@CSAC and H_2O_2 significantly influenced the heat release in the reaction system, underscoring its potential for sustainable and adaptable applications in sewage treatment processes.

Introduction

Energy and environmental protection are two pivotal areas of human research; however, various emissions from energy consumption pollute the environment, and environmental treatment requires a substantial amount of energy. Energy recovery can maximize the protection and prolong the life of natural resources, reduce the pollution of air and water resources, reduce greenhouse gas emissions, and reduce energy costs. All these factors are important elements for protecting natural resources and the environment, and for economic efficiency. While technologies such as waste incineration[1,2] and biogas fermentation[3,4] are used widely for this purpose, relevant research and applications of the heat generated during the treatment of sewage are lacking.

Sewage-source heat pumps primarily utilise sewage as both cold and heat sources to extract and store energy. Such systems achieve a heating effect through the physical cycle change of the refrigerant within the heat pump unit system, thereby consuming a minimal amount of electric energy. Accordingly, this method has significant implications for utilising sewage and low-grade clean energy.[5,6] Considering the optimal energy consumption of the sewage extraction heat process, the temperature typically decreases after sewage extraction by approximately 4 °C.[7] Therefore, investigating technology that generates by-product heat energy during sewage treatment and the resultant increase in temperature holds great significance. This capability could potentially double the heat output of the

Engineering Training Center, Shandong University, No. 27, South Shanda Road, Jinan, Shandong Province, China. E-mail: yanyuntao@sdu.edu.cn

sewage-source heat pump, proving valuable for energy recovery and utilising the sewage treatment process.

The aromatic compound *O*-phenylenediamine is used widely in pharmaceuticals, pesticides, dyes, and tobacco smoke. It is also widely prevalent in various sewage types, posing a significant risk for contaminating both ground and surface water.[8] Moreover, *O*-phenylenediamine is known to be harmful to humans through consumption, inhalation, or eye exposure.[9] In recent years, Fenton advanced-oxidation technology for the degradation of organic sewage has progressed rapidly.[10] The Fenton oxidation process degrades or even mineralises organic pollutants into non-toxic inorganic substances by generating strong, oxidising free radicals. However, the traditional Fenton reaction only occurs in an acidic environment with low pH, leading to the production of a substantial amount of iron mud. At pH >4.0, Fe^{3+} exists in the form of an insoluble complex, rendering the Fenton reaction impractical and significantly reducing the pollutant removal rates. Consequently, using the Fenton method for sewage treatment often requires acidification pretreatment, increasing treatment costs and limiting its practical application.[11] In recent years, heterogeneous Fenton catalytic oxidation has advanced swiftly, solidifying free metal ions to create metal, metal oxide, metal-supported, and metal-ion-doped solid catalysts.[12–14] The heterogeneous Fenton catalyst has high stability, adjustable structure, certain chemical inertness, and good electrical properties,[15] increasing the reaction site and reducing catalyst leaching. This catalyst offers advantages such as a wide pH response range, no secondary pollution, and easy separation of active components. For example, Wu *et al.* used mechanical activation treatment combined with high-temperature pyrolysis to prepare Fe₃O₄

magnetic nanocomposites with strong degradation of tetracycline hydrochloride and a 2.4-fold increase in the initiation rate constant compared with that of dark conditions.[16] Uttam et al. investigated the photo-Fenton PNP degradation performance of $Ag/Fe_3O_4/WO_3$ photocatalysts. These authors used classical MD simulations to predict the effective interaction of H_2O_2 with Fe_3O_4 photocatalysts and measured the Ag loading for optimal degradation activity.[17] Van Pham et al. investigated how diatomaceous earth could be used to remove ciprofloxacin (CIP) in a photo-Fenton system, with the catalytic degradation rate reaching 90.03%, with 80% still being achieved after five cycles.[18] Further, Xu et al. used the original iron-containing clay as a Fenton catalyst to study the degradation reaction of phenol in water, achieving a degradation efficiency of more than 90%.[19] Zhang et al. prepared copper-loaded molecular sieve catalysts to completely remove methylene blue dye in a Fenton system within 90 min.[20] Cui et al. successfully prepared Co–N codoped carbon nanotubes (Co–N-CNTs), demonstrating rapid degradation efficiency and reusability for degrading Rhodamine B(RhB).[21] Hammad et al. studied the preparation method of iron oxide/graphene nanostructures. Their findings included high degradation efficiency for organic pollutants, indicating optimal stability in a wide pH range (from 3 to 9).[22] However, existing heterogeneous Fenton catalysts suffer from complex production processes or high production costs. Such disadvantages have led to a growing focus on researching catalyst carriers with lower cost or simpler production processes.

Biochar has been applied progressively in remediating environmental pollution because of its excellent porosity, low production cost, and strong adsorption capacity for organic pollutants and heavy metals.[23,24] Coconut shell, an abundant tropical agricultural waste, is a sustainable resource for producing coconut shell-activated carbon (CSAC) through heat treatment. The CSAC has a high microporous structure, excellent specific surface area, and a variable pore structure,[25] making it a good choice as a catalyst carrier. For instance, Higai et al. studied the factors influencing the saccharification process of cellulose by coconut shell-activated carbon.[26] Halepoto et al. investigated the SCR reaction of NO on Fe-loaded CSAC, achieving a remarkable 95% reduction rate for NO.[27] Trisunaryanti et al. explored the characteristics of CSAC, prepared under different activation conditions as Ni and Pt catalyst supports for catalytic hydrogenation of naphtha to hydrocarbon biofuels, yielding higher liquid products.[28] However, no research has been reported on the heat release law of the heterogeneous Fenton system with CSAC as the carrier for sewer degradation.

In the current study the heat release characteristics of multiphase Fenton under optimal degradation conditions were explored. A heterogeneous Fenton-like catalyst, $Fe_3O_4@CSAC$, was prepared by loading Fe_3O_4 on CSAC, and the degradation performance and heat release characteristics of o-phenylenediamine-simulated sewage was explored using this system. $(Fe_3O_4@CSAC)–H_2O_2$ heterogeneous Fenton-like. The current study established a theoretical foundation for addressing the existing challenges in Fenton technology and promoting energy utilisation in sewage treatment. The research, therefore, contributes positively to reducing petrochemical energy consumption and protecting the environment.

Experiments

Instruments

Thermostatic water bath (HWS-26, Shenzhen Yice Medical Testing Technology Co., Ltd, China); pH analyser (HFPD, Wuxi Haines Automation Instrument Co., Ltd, China); temperature recorder (LORA, Jinan Renshuo Electronic Technology Co., Ltd, China); chemical oxygen demand (COD) tester (LB-901A, Qingdao Lubo Jianye Environmental Protection Technology Co., Ltd, China); electric stirrer (OS20-S, Shanghai Kexing Instrument Co., Ltd, China); precision balance (FA1204B, Qingdao Juchuang Environmental Protection Group Co., Ltd, China); vacuum tube furnace (GS1200-80, Hebei Yagelon Technology Co., Ltd, China); Fourier transform infrared spectrometer (Nicolet 6700, ThermoFischer Scientific, Massachusetts, USA); field emission scanning electron microscope [Quanta 400 FEG, Field Electron and Ion Company (FEI), Oregon, USA]; and X-ray diffractometer (SmartLab 3KW, Rigaku, Japan).

Pharmaceuticals

98% H_2SO_4, NaOH, 30% H_2O_2, Ag_2SO_4, $Fe(NH_4)_2 \cdot (SO_4)_2 \cdot 6H_2O$, $C_6H_8N_2$, $K_2Cr_2O_7$, $FeSO_4$, and $Fe_2(SO_4)_3$ (Guoyao Group Chemical Reagents Co., Ltd, China; CSAC, Zhengzhou Sewage Treatment Materials Co., Ltd China). All chemical reagents were analytical pure grade at least.

Catalyst production

NaOH solution was prepared as 3 mol L^{-1}, and 500 g CSAC was added. After soaking for 24 h, it was strained and washed. The samples were immersed in 1.0 mol L^{-1} H_2SO_4 solution, rinsed again after 24 h, and the modified CSAC was obtained after 12 h of drying at 200 °C.

To ensure a ratio of 0.8 mol L^{-1} : 0.4 mol L^{-1} : 500 g between Fe^{3+}, Fe^{2+}, and CSAC for the preparation process, a mixed solution including 0.4 mol L^{-1} $Fe_2(SO_4)_3$ with 0.4 mol L^{-1} $FeSO_4$ was prepared. Subsequently, 500 g of the modified CSAC was introduced into the mixed solution with continuous stirring. After 24 h, the sample was transferred into a beaker. Afterwards, a solution of 0.6 mol L^{-1} NaOH was poured into the beaker and the sample was submerged for 2 h. Subsequently, the samples were filtered, washed with ultrapure water, and the $Fe_3O_4@CSAC$ catalysts were obtained after 2 h in a vacuum tube furnace at 500 °C.

Experimentation

As shown in Fig. 1, the reaction was conducted inside a 500 mL round-bottomed flask, with the outer walls of the flask wrapped with an insulating layer. The blades of the stirrer and the temperature probe inside the flask were connected to the controller outside the flask through the flask mouth. The stirrer controlled the rotational speed and the temperature recorder automatically recorded the temperature value. Laboratory ambient temperature of 25 °C, three times measured at 60 °C,
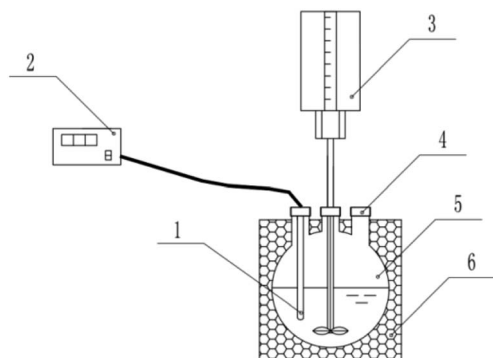
Fig. 1 Diagram of experimental device temperature probe (1), temperature recorder (2), stirrer (3), drug inlet (4), reaction dish (5), and thermal barrier (6).

simulated sewage in the preheating treatment of the experimental setup in 180 min after the temperature reduction value was less than 0.6 °C. The accuracy of the temperature measurements was ensured in this way.

Pharmaceutical preparation

Different concentrations of *o*-phenylenediamine solution, 0.05 mol L^{-1} H$_2$SO$_4$, and 0.1 mol L^{-1} NaOH were prepared in volumetric flasks with ultrapure water. *O*-Phenylenediamine solution was used to simulate sewage samples, and the H$_2$SO$_4$ and NaOH solutions were used to change the pH of the simulated sewage.

Experimental procedure

The volumetric flask with simulated sewage was placed in a thermostatic water bath to raise the temperature of the simulated sewage to 10 °C above the initial reaction temperature. Afterwards, a measured quantity of Fe$_3$O$_4$@CSAC catalyst and preheated simulated sewage were added to the flask (Fig. 1). The stirrer was activated, with the rotational speed set to 600 rpm. The temperature recorder was turned on to monitor the internal temperature of the flask. Once the internal temperature reached the initial reaction temperature, a fixed amount of H$_2$O$_2$ solution was injected into the flask, and the reaction start time was recorded. The reaction continued for 180 min and, after filtration, the COD value of the reaction solution was measured.

Default reaction conditions: initial reaction temperature 30 °C, concentration of *o*-phenylenediamine solution 0.04 mol L^{-1}, concentration of H$_2$O$_2$ 0.25 mol L^{-1}, amount of Fe$_3$O$_4$@CSAC 532 g L^{-1}, and pH of 7.1. All experiments were replicated three times. The data presented in the conclusion and analysis sections of the manuscript are the average of the data from the three experiments, the error bars on the graphs are the maximum data difference between the three experiments, and the data points are connected by a spline curve. The experimental data were processed using Origin2018 and Excel2019 software for statistical analysis. The COD degradation rate of the reaction solution is expressed by η, the degradation amount

is expressed as ΔC, and the increase in solution temperature during the reaction process is expressed as ΔT, calculated as shown in eqn (1)–(3). Where C is the COD value after the reaction, C_0 is the initial COD value, T is the maximum temperature of the reaction, and T_0 is the initial temperature.

$$\eta = \Delta C / C_0 \times 100\% \tag{1}$$

$$\Delta C = C_0 - C \tag{2}$$

$$\Delta T = T - T_0 \tag{3}$$

Results and discussion

XRD analysis

Fig. 2 shows the XRD spectrum of the Fe$_3$O$_4$@CSAC sample. New diffraction peaks at $2\theta = 62.6°$, 57.0°, 35.5°, and 30.1° occurred on the Fe$_3$O$_4$@CSAC sample (Fig. 2). Compared with the Fe$_3$O$_4$ standard card (JCPDF No. 88-0866), the Fe$_3$O$_4$ in the sample was in an equiaxed magnetite phase,[29] indicating that Fe$_3$O$_4$ successfully loaded to the CSAC carrier surface.

Fourier transform infrared spectroscopy (FTIR) analysis

The FTIR test results are shown in Fig. 3. The O–H stretching vibration peak appeared at 3431.225 cm^{-1},[30,31] the C=O and aryl ring stretching vibration peak at 1732.727 cm^{-1} and 1560.612 cm^{-1},[30,31] the C–C stretching vibration peak at 1093.923 cm^{-1},[29] and the vibration peak at 791.154 cm^{-1}, indicating that the CSAC possesses a C–H bond.[32,33] A stretching vibration peak at 587.700 cm^{-1} was observed on the Fe$_3$O$_4$@CSAC material, and the absorption peak here represented the Fe–O vibration in Fe$_3$O$_4$,[34] indicating that iron on Fe$_3$O$_4$@CSAC mainly existed in the form of Fe$_3$O$_4$.

XPS analysis

The X-ray photoelectron spectroscopy (XPS) test results of the Fe$_3$O$_4$@CSAC sample are shown in Fig. 4. Fig. 4(a) shows the
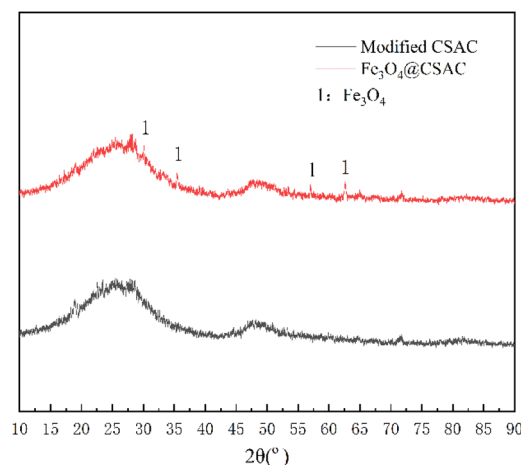
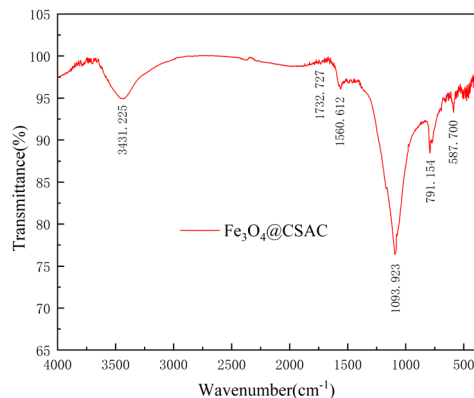

Fig. 2 XRD patterns of modified CSAC and Fe$_3$O$_4$@CSAC.

Fig. 3 FTIR images of $Fe_3O_4@CSAC$.

Fe_{2p} spectrum fitted into five single peaks, where the binding energies of 709.5 eV and 723.1 eV corresponded to Fe^{2+}, the binding energies of 711.8 eV and 725.8 eV corresponded to Fe^{3+}, and the satellite peak was at binding energy 718.1 eV. These results confirmed the presence of both Fe^{3+} and Fe^{2+} in $Fe_3O_4@CSAC$,[35] with the ratio of Fe^{3+} to Fe^{2+} being approximately 2 : 1. The preparation agent of $Fe_3O_4@CSAC$ is analytically pure with high purity, and no oxidizing and reducing agents were added in the preparation process. Accordingly, it could be assumed that no change occurred in the valence states of Fe^{3+} and Fe^{2+} in the material. Moreover, as indicated in Fig. 4, it could be concluded that the amount of catalyst-loaded Fe^{3+} and Fe^{2+} conformed to the additive ratio. It could be assumed that the two main forms of Fe^{3+} and Fe^{2+} were on the catalyst, and
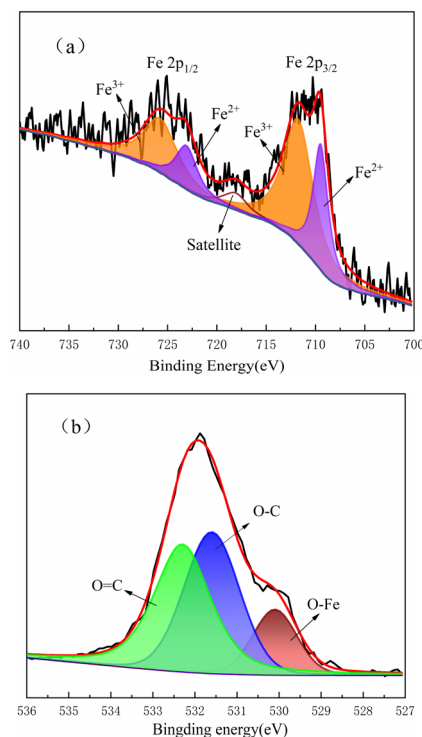
the content and effects of other valence states were almost negligible. Fig. 4(b) shows the O 1s spectrum. The binding energy of 530.1 eV belonged to the O–Fe of Fe oxides, while the binding energies of 531.6 eV and 532.3 eV belonged to O=C and O–C, respectively.[36]

Scanning electron microscopy (SEM) analysis

Fig. 5 is a SEM image of CSAC, modified CSAC, and $Fe_3O_4@$-CSAC. A comparison between Fig. 5(a) and (b) revealed that the surface impurities of CSAC were significantly reduced after modification treatment, unblocking of pores, and showing an evident pore structure. The pores of the modified CSAC were developed and arranged regularly. Fig. 5(c) shows the SEM image of $Fe_3O_4@CSAC$, indicating the uniform dispersion of Fe_3O_4 particles on the carrier surface. The flat and regular surfaces of the treated CSAC enhanced the dispersion degree of active ingredients, prevented the metal particles from agglomerating, and contributed to improving catalytic activity.
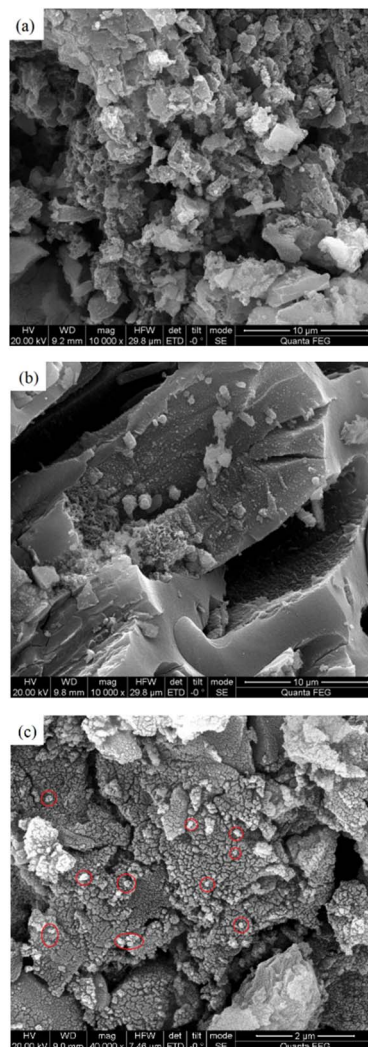

Fig. 4 XPS images of $Fe_3O_4@CSAC$ Fe 2p (a), and O 1s (b).

Fig. 5 SEM images of CSAC, modified CSAC, and $Fe_3O_4@CSAC$ CSAC (a), modified CSAC (b), and $Fe_3O_4@CSAC$ (c).

Effect of catalyst dosage

The impact of the Fe_3O_4@CSAC catalyst dosage on the oxidative degradation of o-phenylenediamine in the (Fe_3O_4@CSAC)–H_2O_2 heterogeneous Fenton-like system is shown in Fig. 6. The addition of Fe_3O_4@CSAC was adjusted to 133 g L^{-1}, 266 g L^{-1}, 399 g L^{-1}, 532 g L^{-1}, and 665 g L^{-1}, respectively.

Fig. 6 also shows that ΔT and η increased along with the increase in the Fe_3O_4@CSAC catalyst dosage. When the Fe_3O_4@CSAC dosage was below 266 g L^{-1}, both ΔT and η exhibited substantial growth. When the Fe_3O_4@CSAC dosage exceeded 266 g L^{-1}, the rate of increase in ΔT and η diminished. This trend was attributed to the relationship between ΔT and η and the concentration of ˙OH.[37] When the dosage of Fe_3O_4@CSAC was less than 266 g L^{-1}, owing to insufficient Fe_3O_4@CSAC, the catalytic speed of H_2O_2 decomposition into ˙OH was slow. As the dosage increased, the number of active sites within the system increased, accelerating the decomposition of H_2O_2 into ˙OH. This occurrence increased the total amount of reaction in the solution, and increased the heat release and degradation of o-phenylenediamine molecules. These phenomena resulted in the rapid escalation of both ΔT and η. However, when the dosage of Fe_3O_4@CSAC exceeded 266 g L^{-1}, the Fe_3O_4@CSAC amounts were excessive, considering both the concentration of H_2O_2. In this scenario, the presence of ˙OH in the solution was limited primarily by the concentration of H_2O_2. Despite the augmented active sites following the increased Fe_3O_4@CSAC dosage, the inadequate concentration of H_2O_2 prevented the catalyst from adsorbing more H_2O_2. Consequently, the production of ˙OH declined, leading to a decline in both ΔT and η.

The degradation of the simulated sewage, catalysed by H_2O_2 and Fe_3O_4@CSAC, was speculated to follow the following steps. (1) H_2O_2 and O-phenylenediamine molecules of the reaction solution were adsorbed on the surface or pores by Fe_3O_4@CSAC. (2) The adsorbed H_2O_2 was decomposed into radicals such as ˙OH by the catalytic action of the active sites on the surface of the Fe_3O_4@CSAC catalyst. (3) Free radicals such as ˙OH reacted with the adsorbed o-phenylenediamine molecules. (4) The amount of the degradation products increased and they were gradually desorbed from the catalyst surface into the solution.
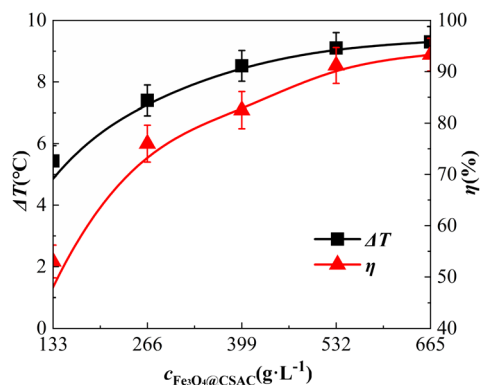
(5) As the number of o-phenylenediamine molecules and H_2O_2 on the surface of Fe_3O_4@CSAC catalyst decreased, the o-phenylenediamine molecules and H_2O_2 in the solution continued to be adsorbed onto the catalyst, establishing a cyclic process of catalytic degradation. The data presented in Fig. 6 indicated that ΔT and η exhibited similar patterns; moreover, elevating η by increasing the catalyst dosage increased the ΔT of the solution.

Effect of H_2O_2 dosing concentration

The impact of the H_2O_2 dosage concentration is shown in Fig. 7. The dosage concentrations of H_2O_2 were 0.05 mol L^{-1}, 0.10 mol L^{-1}, 0.15 mol L^{-1}, 0.20 mol L^{-1}, 0.25 mol L^{-1}, and 0.30 mol L^{-1}, respectively.

Fig. 7 shows a rapid increase in η when the H_2O_2 dosage increased from 0.05 mol L^{-1} to 0.15 mol L^{-1}. When the amount of H_2O_2 continued to increase, the increase in η declined, and when the amount of H_2O_2 increased to 0.25 mol L^{-1}, η reached 91.2%. Notably, when the amount of H_2O_2 was raised further to 0.30 mol L^{-1}, η was reduced slightly to 90.5%. This result is consistent with the observation by Zhang $et\ al.$ in a study on BAC degradation.[38] This phenomenon occurs when the concentration of H_2O_2 is relatively low and nearly all the free radicals, such as ˙OH catalytically decomposed by H_2O_2, are used to degrade o-phenylenediamine molecules. As a result, η increased significantly along with an increase in the H_2O_2 concentration. With an escalating H_2O_2 concentration, more H_2O_2 molecules were adsorbed on the surface of the catalyst, occupying its adsorption sites to a certain extent. H_2O_2 decomposed numerous ˙OH and other free radical molecules on the surface of the catalyst, fully degrading the adsorbed o-phenylenediamine molecules; however, after degradation, the o-phenylenediamine molecules in the solution had not been adsorbed. Consequently, a quenching reaction occurred between ˙OH and other free radicals. Therefore, as the H_2O_2 dosage concentration increased, the rise in η slowed down. When the quenching reaction became more prevalent, η appeared to decrease.
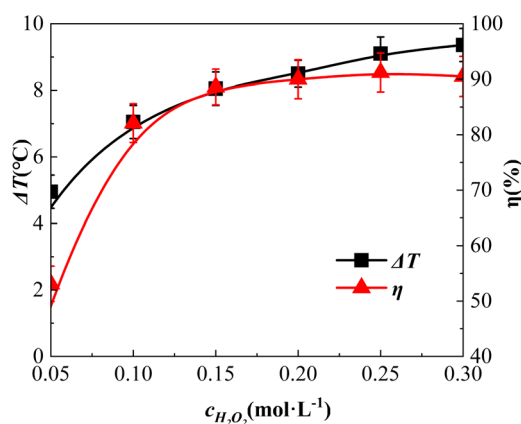

Fig. 6   Effect of catalyst addition measurement on η and ΔT.

Fig. 7   Effect of H_2O_2 dosage concentration on η and ΔT.

Fig. 7 shows that ΔT increased from 4.9 °C to 9.4 °C when the H_2O_2 dosage was increased from 0.05 mol L^{-1} to 0.3 mol L^{-1}, which differs from the pattern of η initially increasing and then decreasing along with the rise in H_2O_2 concentration. Further, ΔT increased continuously. This deviation was ascribed to the following: at low H_2O_2 concentrations, $\cdot$OH and other free radicals in the solution mainly reacted with o-phenylenediamine molecules, with the reaction being exothermic. As the concentration of H_2O_2 continued to increase, the reactions of $\cdot$OH and other free radicals with o-phenylenediamine molecules increased, thereby increasing ΔT. Subsequently, as the concentration of H_2O_2 continued to increase, the excess $\cdot$OH and other free radicals produced by catalytic H_2O_2 were quenched (an exothermic reaction). As ΔT was linked to the amount of $\cdot$OH and other free radicals produced by catalytic decomposition,[37] it continued to rise along with the increasing H_2O_2 concentration.

Considering that the degradation process occurred mainly at the catalyst surface, the free radicals such as $\cdot$OH generated in the system resulted from catalytic H_2O_2 catalysed by Fe^{2+} in the active site of the catalyst [eqn (4)]. Concurrently, Fe^{2+} was oxidised to Fe^{3+} and, as the reaction proceeded, Fe^{2+} had to undergo the reaction [eqn (5)] to be regenerated in a cyclic manner.[39] The reaction rate constant of eqn (5) is $k = 0.02$ L mol^{-1} s^{-1}, *i.e.*, smaller than that of eqn (4), $k = 76$ L mol^{-1} s^{-1}.[37] With the increase of the H_2O_2 dosing concentration, the reaction system with high H_2O_2 dosing concentration showed a rapid reaction rate in the early stage. As the reaction proceeded, the catalytic generation of $\cdot$OH radicals was constrained by the reaction shown in eqn (5), and the generation rate decreased rapidly. Moreover, the difference in the reaction rate and the reaction system with a low dosing concentration of H_2O_2 decreased gradually, thereby gradually reducing the increase in ΔT.

$$Fe^{2+} + H_2O_2 \rightarrow Fe^{3+} + \cdot OH + HO^- \qquad (4)$$

$$Fe^{3+} + H_2O_2 \rightarrow Fe^{2+} + HO_2\cdot + H^+ \qquad (5)$$
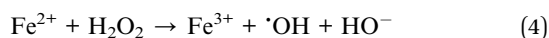
As shown by eqn (4), $\cdot$OH is produced mainly by H_2O_2 catalysed by the Fe^{2+} active site; therefore, it could be concluded that Fe^{2+} was the main active site that catalyses the production of $\cdot$OH from H_2O_2. Further, Fe^{2+} was converted to Fe^{3+} and then had to be reduced to Fe^{2+} [eqn (5)], after which it continued to catalyse the decomposition of H_2O_2 to produce $\cdot$OH. However, the slower reaction rate [eqn (5)] constrained the reduction of Fe^{2+} and affected the rate of $\cdot$OH radical production. Accordingly, the Fe^{3+} active site on $Fe_3O_4@CSAC$ had a favourable effect on the efficiency of the catalyst redox cycle.

Effect of initial reaction temperature

Fig. 8(a) shows the impact of the initial reaction temperature. The initial reaction temperatures were adjusted to 10 °C, 20 °C, 30 °C, 40 °C, 50 °C, and 60 °C, respectively. Fig. 8(b) shows the COD values of 0.04 mol L^{-1} o-phenylenediamine solution held at different temperatures for 180 min. As shown, the COD was almost the same at different temperatures, and it could be
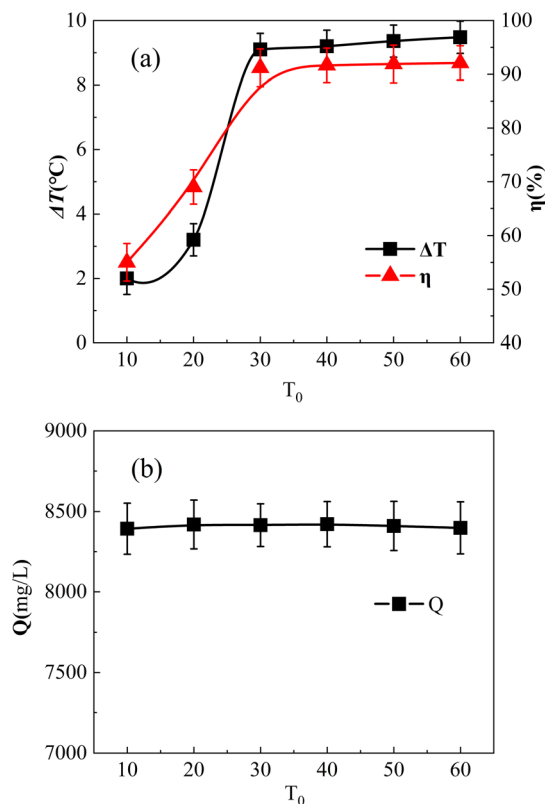

Fig. 8 Effect of initial reaction temperature on η and ΔT. Effect of T_0 on η and ΔT (a), and effect of T_0 on Q (b).

assumed that o-phenylenediamine would not decompose in a limited temperature change environment. Moreover, it could be assumed that the initial temperature change in the experiment mainly affected the degradation of o-phenylenediamine by the $(Fe_3O_4@CSAC)$–H_2O_2 reaction system.

Fig. 8(a) shows that the initial reaction temperatures of 10 °C and 20 °C led to a low η, which increased rapidly from 20 °C to 30 °C, but ceased to increase after the temperature exceeded 30 °C. This reaction was ascribed the molecular activity in the solution being low when the temperature was low, which reduced the production of $\cdot$OH and other free radicals. Therefore, the amount of reaction per unit time to degrade o-phenylenediamine molecules was minimal, leading to low η. As the initial reaction temperature increased, the molecular activity increased rapidly, the adsorption and reaction rate of the catalyst accelerated, and η increased rapidly. However, when the temperature exceeded 30 °C, the amount of adsorbed and decomposed o-phenylenediamine and H_2O_2 did not increase, and η ceased to increase at constant initial o-phenylenediamine and H_2O_2 concentrations.

As shown in Fig. 8(a), ΔT increased along with the rise in the initial reaction temperature. At 10 °C and 20 °C, ΔT was comparatively low, measuring 2 °C and 3.2 °C, respectively. This reaction was ascribed to the reduced molecular activity at lower initial reaction temperatures, which inhibited catalyst adsorption and catalytic decomposition of H_2O_2. The lower total amount of $\cdot$OH resulted in a smaller total heat release, leading to a temperature rise that was less substantial. At a temperature

exceeding 30 °C, ΔT increased slightly, unlike the pattern of η ceasing to increase. This phenomenon was ascribed to the total amount of material in the reaction system remaining constant. The total amount of *o*-phenylenediamine molecules and H_2O_2 adsorbed on the surface and pores of the catalyst remained the same; however, the higher the molecular activity the faster would be the catalytic decomposition. Moreover, degradation could occur on the surface of the catalyst and in the pores, and more heat could be released per unit time. As the reaction occurred on the surface of the catalyst and inside the pores, the overall warming of the solution was diffused to the solution from the surface and inside the catalyst. The reason for this is that heat conduction follows a specific process, and the higher the local temperature was the faster would be the heat conduction. Consequently, a higher local temperature would accelerate the diffusion of heat to the overall solution, with the measured ΔT rising higher.

Furthermore, as shown in Fig. 8(a), the initial reaction temperature increased from 10 °C to 20 °C and, afterwards, to 30 °C. The difference in the magnitude of the increase in solution η was small and almost proportional. This occurrence was ascribed to a higher initial reaction temperature enhancing molecular activity and promoting the adsorption of *o*-phenylenediamine and H_2O_2 molecules by the catalyst. With more *o*-phenylenediamine molecules and H_2O_2 adsorbed per unit time, fewer *o*-phenylenediamine molecules remained in the solution, resulting in an increase in η. This finding indicated the direct impact of the initial reaction temperature on the catalytic rate and adsorption performance of Fe₃O₄@CSAC. The temperature increase in the solution was lower under reaction conditions with an initial reaction temperature below 20 °C. This was ascribed to the slow catalytic degradation reaction of *o*-phenylenediamine molecules and H_2O_2 adsorbed on the catalyst surface at lower overall temperatures, which limited the reaction heat per unit time. Local heat diffusion to the solution was a gradual process, resulting in the system temperature rising slowly, as well as a slight ΔT.

As a higher sewage temperature leads to higher energy recovery, a lower sewage temperature affects the energy recovery efficiency to a certain extent. In engineering applications, a double degradation tank could be set up for the initial low temperature, with the release of heat from the outer degradation tank used mainly to heat the inner degradation tank. Further, the sewage source pumps mainly recycled the inner degradation tank heat energy; therefore, this method compensated for the sewage temperature being too low and almost unable to recover the heat.

Effect of solution pH

The influence of the initial pH value is shown in Fig. 9. The initial pH values of the reaction solution were adjusted to 3.1, 5.1, 7.1, 8.9, and 11.0, respectively.

As shown in Fig. 9, the η of *o*-phenylenediamine decreased from 93.2% to 76.4% as the pH value increased from 3.1 to 11.0. Under acidic conditions, with the gradual increase of the pH value, η decreased from 93.2% to 91.2%, η decreased by 2%, η
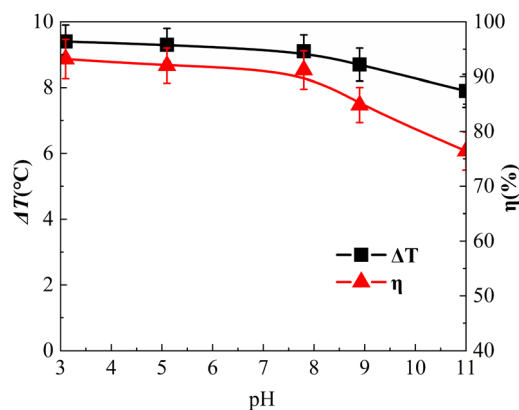

Fig. 9 Effect of pH on η and ΔT.

only decreased slightly and remained at a high level. These results were attributed to the presence of H^+ under acidic conditions preventing the decomposition of H_2O_2 into HOO^-, which is a hydroxyl radical scavenger that has a strong scavenging effect on ·OH. Acidic conditions are conducive to the catalytic decomposition of H_2O_2 into ·OH by Fe₃O₄@CSAC. In an alkaline environment, pH increased from 7.1 to 11.0, η decreased from 91.2% to 76.4%, and η decreased by 14.8%. It could be concluded that alkaline conditions had a certain inhibitory effect on the degradation of *o*-phenylenediamine by the (Fe₃O₄@CSAC)–H_2O_2 heterogeneous Fenton-like system. The probable reasons for this result were as follows. On the one hand, with alkaline pH, H^+ was consumed by OH^- in the solution, which promoted the hydrolysis of H_2O_2 to HOO^-. Moreover, a large amount of H_2O_2 was consumed, resulting in a decrease in the concentration of ·OH. On the other hand, the CO_2 produced by degradation easily converted into CO_3^{2-} and HCO_3^- in alkaline solution, CO_3^{2-} and HCO_3^- can react with ·OH to form CO_3^-, and the two ions consumed a large amount of ·OH ions(k(·OH, CO_3^{2-}) = 3.9 × 108 mol L^{-1} s^{-1}, k (·OH, HCO_3^-) = 8.5 × 106 mol L^{-1} s^{-1}),[40] thereby affecting the degradation of *o*-phenylenediamine by the system.

As shown in Fig. 9(c), when the pH value of the solution increased from 3.1 to 11.0, ΔT decreased gradually. Under acidic conditions, as the pH value gradually increased, ΔT decreased from 9.4 °C to 9.1 °C. Under alkaline conditions, the pH increased from 7.1 to 11.0, ΔT decreased from 9.1 °C to 7.9 °C, and the range pf decrease increased. The impact of acidic conditions on the heat release of the system oxidative *o*-phenylenediamine solution was minimal, and the alkaline conditions had a certain inhibitory effect on the heat release of the system. Compared with the optimal pH value of 2.0–4.0 in the traditional Fenton oxidation process,[41] This was ascribed to the oxidation of Fe^{2+} to Fe^{3+} having to be reduced to Fe^{2+} [eqn (5)], and the reaction in eqn (4) being much faster than that in eqn (5). The catalytic efficiency of the system was probably mainly affected by the speed of the procedure shown in eqn (5), with the (Fe₃O₄@CSAC)–H_2O_2 heterogeneous Fenton-like system demonstrating broader pH adaptability. The reason for this was that the predominant Fe^{2+}/Fe^{3+} conversion occurring on the reaction system mainly occurred on the surface of the catalyst

crystal within the reaction system. This surface-based conversion mitigated the formation of iron ion hydroxide precipitation under high pH conditions, preventing further weakening of the procedure [eqn (5)], and ensuring that the Fe$_3$O$_4$@CSAC catalyst maintained high catalytic activity under neutral or even alkaline conditions. Consequently, the pH adaptation range of the heterogeneous Fenton-like system was extended.

Effect of initial reaction concentration of *o*-phenylenediamine

The effect of *o*-phenylenediamine concentration in the reaction solution is shown in Fig. 10. The *o*-phenylenediamine concentrations of the reaction solution were adjusted to 0.01 mol L^{-1}, 0.02 mol L^{-1}, 0.03 mol L^{-1}, 0.04 mol L^{-1}, 0.05 mol L^{-1}, and 0.06 mol L^{-1}, respectively.

As shown in Fig. 10(a), the degradation amount (ΔC) of *o*-phenylenediamine increased along with the increasing *o*-phenylenediamine concentration. Below 0.04 mol L^{-1}, ΔC exhibited a proportional increase, indicating excessive concentrations of *o*-phenylenediamine and Fe$_3$O$_4$@CSAC. Consequently, the catalyst produced abundant free radicals (*e.g.*, ·OH), which facilitated comprehensive degradation of *o*-phenylenediamine, and prompted the ΔC to increase proportionally. Conversely, concentrations above 0.04 mol L^{-1} resulted in a decline in the increase rate of ΔC because of the approaching adsorption saturation of the catalyst. With increased *o*-phenylenediamine concentration, the adsorption rate declined, leading to a decrease in ΔC.
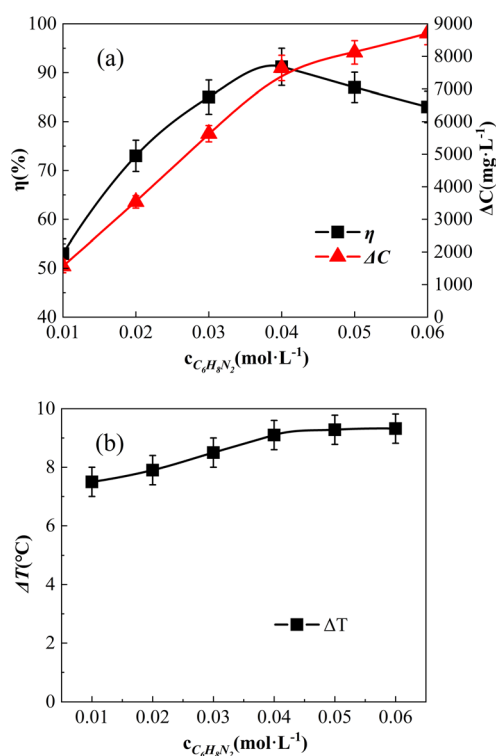
Additionally, Fig. 10(a) shows that η initially increased and then decreased along with the rising *o*-phenylenediamine concentration. This occurrence was ascribed to the degradation reaction occurring on the surface of the catalyst. At lower concentrations of *o*-phenylenediamine, high H$_2$O$_2$ caused substantial aggravation on the catalyst surface, hindering *o*-phenylenediamine adsorption, and resulting in a lower η of *o*-phenylenediamine. As the *o*-phenylenediamine concentration increased, easier adsorption and reaction with ·OH and other free radicals promoted an increase in η. However, upon reaching a critical concentration, constrained by the H$_2$O$_2$ concentration, the degradation amount failed to keep pace with the increased concentration, resulting in a decline in η.

As shown in Fig. 10(b), ΔT increased with the rise in the concentration of *o*-phenylenediamine in the solution. The ΔT rate of increase slowed down at concentrations above 0.04 mol L^{-1}. This trend was attributed to the enhanced concentration degradation of *o*-phenylenediamine at higher concentrations, leading to increased heat release and, consequently, higher solution temperatures. Subsequently, excessive *o*-phenylenediamine molecules in the solution inhibited the adsorption of H$_2$O$_2$ by the catalyst, allowing *o*-phenylenediamine molecules to seize the active site of the catalyst. This occurrence reduced the production of ·OH by Fe$_3$O$_4$@CSAC–catalysed H$_2$O$_2$, and resulted in a smaller increase in the total reaction amount. Solution ΔT was limited by the total amount of reaction in the solution; therefore, only a slight increase in solution ΔT occurred.

Conclusion

The following conclusions were drawn from the results of this study on the degradation performance and heat release characteristics of the (Fe$_3$O$_4$@CSAC)–H$_2$O$_2$ multiphase Fenton-like system.

The Fe$_3$O$_4$ nanoparticles are loaded uniformly on the surface of modified CSAC, predominantly in the presence of Fe^{3+} and Fe^{2+} ions. The modified CSAC enhanced the active site exhibiting a high degradation performance. The degradation process released substantial heat, offering potential for energy recovery in sewage source heat pump applications.

In the (Fe$_3$O$_4$@CSAC)–H$_2$O$_2$ heterogeneous Fenton-like system, increasing the Fe$_3$O$_4$@CSAC dosage improved the degradation rate and heat release of *o*-phenylenediamine sewage. Additionally, increasing the H$_2$O$_2$ concentration initially boosted the degradation rate of *o*-phenylenediamine, which decreased subsequently. An elevated H$_2$O$_2$ concentration effectively enhanced the reaction heat release.

The (Fe$_3$O$_4$@CSAC)–H$_2$O$_2$ heterogeneous Fenton-like system had a relatively high degradation rate and temperature rise under acidic conditions. When pH increased to 11, the degradation rate and temperature rises were 76.4% and 6.9 °C, respectively, indicating pH adaptability beyond the traditional Fenton system.

When the initial reaction temperature of the (Fe$_3$O$_4$@CSAC)–H$_2$O$_2$ heterogeneous Fenton-like system was lower than 30 °C, the total reaction rate was lower, and the degradation rate and

Fig. 10 Effect of [C$_6$H$_8$N$_2$] on ΔC, η, and ΔT effect of [C$_6$H$_8$N$_2$] on η (a) and ΔC; effect of [C$_6$H$_8$N$_2$] on ΔT and ΔC (b).

temperature rise were limited. A significant increase was observed at an initial reaction temperature of 30 °C, with the subsequent temperature rises having a diminishing impact.

An ideal *o*-phenylenediamine concentration is crucial to optimise the degradation rate of the solution and increase the heat release of the system. For example, when the concentration of H_2O_2 was 0.25 mol L^{-1}, the dosage of Fe_3O_4@CSAC was 532 g L^{-1}, pH was 7.1, the initial reaction temperature was 30 °C, with an *o*-phenylenediamine concentration of 0.04 mol L^{-1} yielding the highest degradation rate (91.2%) and temperature rise (9.1 °C).

In conclusion, this study on the degradation performance and heat release characteristics of the (Fe_3O_4@CSAC)–H_2O_2 heterogeneous Fenton-like system holds significant promise for energy recovery and utilisation in sewage treatment processes. The focus of future research will be further improvements of energy recovery. An in-depth study is planned on Fenton degradation of organic matter and the exothermic mechanism of the catalyst preparation method, as well as the ratio of each material. Efficiency will be explored to promote the application of sewage source heat pumps in industrial practice.

Conflicts of interest

There are no conflicts of interest to declare.

Acknowledgements

References

1 P. Verma, O. Jain and A. Gupta, Waste to Energy (WTE) by Incineration: Current and Future Practices in India , *Recent Advances in Mechanical Engineering*, 2021, DOI: **10.1007/978-981-15-8704-7_46**.

2 N. Dadario, G. F. Luis Roberto Almeida, C. P. Cremasco, *et al.*, Waste-to-Energy Recovery from Municipal Solid Waste: Global Scenario and Prospects of Mass Burning Technology in Brazil, *Sustainability*, 2023, **15**(6), 5397.

3 Z. Jin, S. Rong, S. Yanceng, X. Rui, H. Jun, H. Yuanyuan and Z. Hao, Experimental Study on Potential of Biogas Fermentation from Magnolia grandiflora Leaves under Mesophilic Conditions, *Chinese Wild Plant Resources*, 2020, **39**(2), 7–1026.

4 V. M. Polishchuk, S. A. Shvorov, G. V. Krusir and T. S. Davidenko, Increase of the Biogas Output during Fermentation of Manure of Cattle with Winemaking Waste in Biogas Plants, *Problemele Energeticii. Regional.*, 2020, **2**, 123–134.

5 Y. Jian, W. Tan and Q. Liang, Application of sewage source heat pump in domestic hot water system of general hospital, *Water & Wastewater Engineering*, 2023, ch. 2, vol. 49, pp. 103–109.

6 M.-H. Kim, D.-W. Kim, G. Han, *et al.*, Ground Source and Sewage Water Source Heat Pump Systems for Block Heating and Cooling Network, *Energies*, 2021, **14**(18), 5640.

7 W. Ronghua and Y. Liqian, Effect of untreated sewage source heat pump on biochemical sewage treatment, *J. Harbin Inst. Technol.*, 2011, **43**(6), 132–135.

8 Q. L. Guan, Y. Sun, R. Huo, Y. Xin, *et al.*, Cu-MOF Material Constructed with a Triazine Polycarboxylate Skeleton: Multifunctional Identify and Microdetecting of the Aromatic Diamine Family (o,m,p-Phenylenediamine) Based on the Luminescent Response, *Inorg. Chem.*, 2021, **60**(4), 2829–2838.

9 D. Mathivanan, S. K. Tammina, X. L. Wang and Y. L. Yang, Dual emission carbon dots as enzyme mimics and fluorescent probes for the determination of o-phenylenediamine and hydrogen peroxide, *Microchim. Acta*, 2020, **187**, 292.

10 G. Junling, S. Qing, Z. Anlong, W. Chenfeng and Y. Zixin, Application progress of heterogeneous Fenton catalyst in wastewater treatment, *Appl. Chem. Ind.*, 2021, **50**(10), 2866–2872.

11 L. Heng, Y. Zhengfang, W. Peng and B. Xue, Research progress on resource utilization of Fenton oxidation sludge Fenton, *Environ. Prot. Chem. Ind.*, 2022, **42**(6), 654–660.

12 J. Yang, D. Zeng, Q. Zhang, *et al.*, Single Mn atom anchored on N-doped porous carbon as highly efficient Fenton-like catalyst for the degradation of organic contaminants, *Appl. Catal., B*, 2020, **279**, 119363.

13 S. Siyang, W. Dan, Z. Huanxin, C. Yu, W. Xin and Z. Yu, Fabrication of Co-FeOOH/g-C_3N_4 composite and its catalytic performance on heterogeneous photo-Fenton, *Chin. J. Environ. Eng.*, 2020, **14**(12), 3262–3269.

14 H. Ghanbarlou, B. Nasernejad, F. Nikbakht, *et al.*, Synthesis of an iron-graphene based particle electrode for pesticide removal in three-dimensionalheterogeneous electro-Fenton water treatment system, *Chem. Eng. J.*, 2020, **395**, 12505–12519.

15 N. R. Khalid, A. Majid, M. B. Tahir, *et al.*, Carbonaceous-TiO_2 nanomaterials for photocatalytic degradation of pollutants:A review, *Ceram. Int.*, 2017, **43**(17), 14552–14571.

16 C. Wu, T. Guo, Y. Chen, Q. Tian, Y. Zhang, Z. Huang, H. Hu and T. Gan, Facile synthesis of excellent Fe_3O_4@starch-derived carbon Photo-Fenton catalyst for tetracycline degradation: Rapid Fe^{3+}/Fe^{2+} circulation under visible light condition, *Sep. Purif. Technol.*, 2024, **329**, 125174, DOI: **10.1016/j.seppur.2023.125174**.

17 K. Uttam and S. Indrajit, Visible light photo-Fenton degradation of p-nitrophenol on $Ag/Fe_3O_4/WO_3$ nanocomposites: Experimental and molecular dynamics investigations, *J. Environ. Chem. Eng.*, 2023, **11**(6), 111280.

18 V. Van Pham, H. P. P. La, T. Q. Le, *et al.*, Fe_2O_3/diatomite materials as efficient photo-Fenton catalysts for ciprofloxacin removal, *Environ. Sci. Pollut. Res.*, 2023, **30**(12), 33686–33694.

19 J. Xu, X. Yun, L. Meng, Y. Tian, *et al.*, Iron-containing palygorskite clay as Fenton reagent for the catalytic

degradation of phenol in water, *RSC Adv.*, 2021, **11**(47), 29537–29542.

20 M. S. Zhang and X. L. Wang, Preparation of a Gangue-Based X-type Zeolite Molecular Sieve as a Multiphase Fenton Catalyst and Its Catalytic Performance, *ACS Omega*, 2021, **6**(28), 18414–18425.

21 W. Cui, J. Fang, L. Jiaxi, Y. Wan, *et al.*, Fast Degradation of Rhodamine B by In Situ H2O2 Fenton System with Co and N Co-Doped Carbon Nanotubes, *Materials*, 2023, **16**(7), 2606.

22 M. Hammad, P. Fortugno, S. Hardt, *et al.*, Large-scale synthesis of iron oxide/graphene hybrid materials as highly efficient photo-Fenton catalyst for water remediation, *Environ. Technol. Innov.*, 2021, **21**, 101239.

23 N. S. Kamarudin, F. A. Dahalan, M. Hasan, O. S. An, N. A. Parmin, N. Ibrahim, M. Hamdzah, N. A. M. Zain, K. Muda and E. A. Wikurendra, Biochar: A Review of its History, Characteristics, Factors that Influence its Yield, Methods of Production, Application in Wastewater Treatment and Recent Development, *Biointerface Res. Appl. Chem.*, 2022, **12**(6), 7914–7926.

24 Y. Sik Ok, Z. Qianru, J. Linyu, G. Chengcheng, L. Honghong and Y. Sikok, Preparation of modified biochar and its application in environmental remediation, *J. agric. environ. sci.*, 2021, **40**(5), 913–925.

25 R. K. Ahmad, S. A. Sulaiman, S. Yusup, S. S. Dol, M. Inayat and H. A. Umar, Exploring the potential of coconut shell biomass for charcoal production, *Ain Shams Eng. J.*, 2022, **13**(1), 101499.

26 D. Higai, C. Lee, T. Yong, J. Lang and E. W. Qian, Saccharification of cellulose using biomass-derived activated carbon-based solid acid catalysts, *Fuel Process. Technol.*, 2021, **215**, 106738.

27 A. Halepoto, M. Kashif, J. Argue, Y. Su, *et al.*, Preparations and Characterization on Fe Based Catalyst Supported on Coconut Shell Activated Carbon CS(AC) and SCR of NOx-HC, *Catal. Surv. Asia.*, 2020, **24**(2), 123–133.

28 W. Trisunaryanti, K. Wijaya, T. Triyono, N. Wahyuningtyas, S. P. Utami and S. Larasati, Characteristics of coconut shell-based activated carbon as Ni and Pt catalyst supports for hydrotreating *Calophyllum inophyllum* oil into hydrocarbon-based biofuel, *J. Environ. Chem. Eng.*, 2022, **22**(15), 108209.

29 W. Fan, F. Zhao, M. Chen, J. Li and X. Guo, An efficient microreactor with continuous serially connected micromixers for the synthesis of superparamagnetic magnetite nanoparticles, *Chin. J. Chem. Eng.*, 2023, **59**, 85–91.

30 L. Li, J. Chen, Y. Zhang, J. Sun and G. Zou, Ni-Co bimetallic catalysts on coconut shell activated carbon prepared using solid-phase method for highly efficient dry reforming of methane, *Environ. Sci. Pollut. Res.*, 2022, **29**(25), 37685–37699.

31 L. Feng, C. Jieli, D. Shuai, Z. Huanhuan and Z. Hanlu, Dynamic adsorption performance of activated carbon for advanced treatment on phenolic chemical wastewater, *J. Saf. Environ.*, 2023, **23**(7), 2447–2456.

32 Y. L. Pang, Z. X. Law, S. Lim, *et al.*, Enhanced photocatalytic degradation of methyl orange by coconut shell-derived biochar composites under visible LED light irradiation, *Environ. Sci. Pollut. Res.*, 2021, **28**(21), 27457–27473.

33 J. Lin, Y. Zhang, Y. Liu, J. Xia and S. Tong, Structure and properties of biochar under different materials and carbonization temperatures, *Chin. J. Environ. Eng.*, 2016, **10**(6), 3200–3206.

34 B. Chandran, E. Arumugam, S. Narayanan, *et al.*, A low-cost hybrid GQDs/Fe3O4/polypyrrole nanocomposite based chemo-sensor for electrochemical non-enzymatic selective determination of creatinine in biological samples, *Microchem. J.*, 2023, **194**, 109259.

35 X. H. YI, H. D. JI, C. C. Wang, *et al.*, Photocatalysis-activated SR-AOP over PDINH/MIL-88A(Fe) composites for boosted chloroquine phosphate degradation: Performance, mechanism, pathway and DFT calculations, *Appl. Catal., B*, 2021, **293**, 120229.

36 B. Xue, L. Du, J. S. Jin, *et al.*, In situ growth of MIL-88A into polyacrylate and its application in highly efficient photocatalytic degradation of organic pollutants in water, *Appl. Surf. Sci.*, 2021, **564**, 150404.

37 Y. Yan, Y. Mao, C. Ma, *et al.*, Investigation into the Exothermic Laws of Degradation for o-Phenylenediamine-Containing Wastewater by the Fenton Reaction, *J. Environ. Eng.*, 2019, **145**(10), 04019059.

38 Q. Zhang, Y. F. Xia and J. M. Hong, Mechanism and toxicity research of benzalkonium chloride oxidation in aqueous solution by H_2O_2/Fe^{2+} process, *Environ. Sci. Pollut. Res.*, 2016, **23**(17), 17822–17830.

39 Y. Yan, Y. Mao, Y. Dong, *et al.*, Exothermic laws applicable to the degradation of o-phenylenediamine in wastewater via a Fe^{3+}/H_2O_2 homogeneous quasi-Fenton system, *RSC Adv.*, 2019, **9**(45), 26283–26290.

40 C. Gao, J. Wu, S. Ji and Y. Xing, MIL-88A as a heterogeneous photo-Fenton catalyst for the degradation of benzalkonium chloride under visible light: Performance, degradation pathway, and toxicity evaluation, *J. Environ. Chem.*, 2023, **42**(11), 3878–3891.

41 S. Yazici Guvenc and G. Varank, Degradation of refractory organics in concentrated leachate by the Fenton process: Central composite design for process optimization, *Front. Environ. Sci. Eng.*, 2021, **15**, 1–16.